Spatial Rogue Waves in Photorefractive Ferroelectrics

D. Pierangeli,[1,*] F. Di Mei,[1,2] C. Conti,[1,3] A. J. Agranat,[4] and E. DelRe[1]
[1]Dipartimento di Fisica, Università di Roma "La Sapienza", 00185 Rome, Italy
[2]Center for Life Nano Science@Sapienza, Istituto Italiano di Tecnologia, 00161 Rome, Italy
[3]ISC-CNR, Università di Roma "La Sapienza", 00185 Rome, Italy
[4]Applied Physics Department, Hebrew University of Jerusalem, 91904 Jerusalem, Israel
(Received 27 April 2015; published 25 August 2015)

Rogue waves are observed as light propagates in the extreme nonlinear regime that occurs when a photorefractive ferroelectric crystal is undergoing a structural phase transition. The transmitted spatial light distribution contains bright localized spots of anomalously large intensity that follow a signature long-tail statistics that disappears as the nonlinearity is weakened. The isolated wave events form as out-of-equilibrium response and disorder enhance the Kerr-saturated nonlinearity at the critical point. Self-similarity associable to the individual observed filaments and numerical simulations of the generalized nonlinear Schrödinger equation suggests that dynamics of soliton fusions and scale invariance can microscopically play an important role in the observed rogue intensities and statistics.

DOI: 10.1103/PhysRevLett.115.093901 PACS numbers: 42.65.Sf, 05.45.Yv, 42.65.Hw

Processes that lead to long-tail statistics are of great interest in physics because they allow the observation of events with giant amplitudes that would otherwise be truly rare and unobservable in systems that follow standard distributions. This typically occurs in phenomena that manifest complex dynamics, such as in the appearance of earthquakes in plate motion or in large-scale breakdowns in networks. Long-tail statistics are also observed in waves, in which case the giant perturbations with extreme amplitudes are known as "rogue waves." Originally studied in ocean dynamics, they have now been observed in a variety of different wave-supporting systems where, however, their origin and properties are largely unknown [1–3]. In particular, long-tail statistics have been observed in optical systems, from nonlinear light pulse propagation in optical fiber [4–7] to dissipative cavities [8–11]. In the latter, a key role in rogue wave formation in the temporal domain seems to be played by the onset of a chaotic, turbulent, and unstable dynamics [12,13]. Interestingly, also in spatially extended systems, instabilities have been shown to lead to rogue events in the transverse plane of the optical light beam [14–18]. Here, the presence of blocked or induced disorder [14] or, generally speaking, of an interplay between a nonequilibrium state and a nonlinear mechanism [15], appears a crucial ingredient to extreme event generation, providing interaction and coupling of different spatial regions [16]. Recent findings have further highlighted the role of randomness showing that, even in the apparent absence of a nonlinearity, random field synchronization can trigger the onset of extreme spatiotemporal events [19].

The central role of disorder seems to rule out rogue waves in systems that form the technological basis of photonics, that is, optical crystals with χ_2, χ_3, and photorefractive response, since a stochastic component is in principle absent [20]. To date, no rogue waves have ever been detected in any of these crystals. Considering photorefractives, disorder is known to play a minor role in light dynamics in standard crystal phases [21]. In turn, recent experiments have shown that when a photorefractive ferroelectric is supercooled to its Curie point, long-range fluctuations lead to a transient out-of-equilibrium state characterized by reorienting polar nanoregions that affect light through a strongly enhanced electro-optic response capable of supporting scale-free optics and antidiffraction [22–26]. In these conditions, characterized by disorder and nonlocality in light self-interaction, the complexity of multisoliton spatial dynamics has also been predicted [27].

In this Letter we observe spatial rogue waves in photorefractive crystals of potassium-lithium-tantalate-niobate (KLTN) [28]. The localized and anomalously intense light spots form when the crystal is biased at the ferroelectric phase transition, where optical Kerr-saturated nonlinear propagation is affected by huge stochastic response. The extreme-amplitude events belong to a long-tail statistics and are detected only as the crystal is kept at its critical point. Rogue waves become unobservable as the nonlinearity is weakened, and this suggests that, in our system, it is the combination of disorder and giant nonlinearity that triggers the onset of the normally ultrarare perturbations.

Light propagation at the phase transition is investigated focusing cylindrical Gaussian beams ($\lambda = 532$ nm, $P = 0.1$ mW, FWHM $= 8$ μm) on a photorefractive nanodisordered crystal of KLTN, $K_{1-\alpha}Li_{\alpha}Ta_{1-\beta}Nb_{\beta}O_3$, with $\alpha = 0.04$ and $\beta = 0.38$, illuminated through uniform background intensity I_b. The zero-cut optical quality specimen is $2.4^{(x)} \times 2.0^{(y)} \times 1.7^{(z)}$ mm sized and presents the paraelectric to ferroelectric phase transition at the

room-temperature Curie point $T_C = 294$ K, measured and characterized using low-frequency dielectric spectroscopy. In our experiment, we keep the KLTN crystal at $T = T_C + 1$ K through a Peltier junction; then, an external static electric field is applied along the x direction, parallel to the polarization of the propagating beam [Fig. 1 (left)], via an applied voltage $V = 500$ V. In the proximity of T_C, an electric field larger than the coercive field is able to induce ferroelectric ordering (field-induced transition) [29–31]. The crystal manifests a temperature gradient in the vertical y direction caused by the setup geometry [as in Fig. 1 (left) the Peltier junction is placed on the bottom facet and the thermal capacity is large in proximity of T_C]. Launching a z-directed beam with a spatial extension in the y direction hence allows the inspection of light propagation for different temperature regimes in a single experiment. The nonlinear beam propagation is explored detecting the transmitted beam intensity distribution through an imaging system and a CCD camera. Results indicate a strong dependence on the local temperature. In fact, the spatial scale of the thermal gradient (≈ 300 μm) is such that three qualitatively different regimes of light propagation can be identified, as shown in Fig. 1 (right). When the crystal is warmer the bias field is too weak to induce the ferroelectric transition and the local phase remains paraelectric; here modulation instability associated with the strong photorefractive response governs nonlinear dynamics, breaking, along the initially symmetric y direction, the beam into a periodic pattern of $(2 + 1\text{D})$ beams and inhibiting $(1 + 1\text{D})$ soliton formation [32–34] [Fig. 1(a)]. When the crystal is slightly colder, ferroelectric ordering occurs and light transmission is inhibited by critical opalescence [Fig. 1(c)]. Between these two conditions we find propagation associated with the coexistence

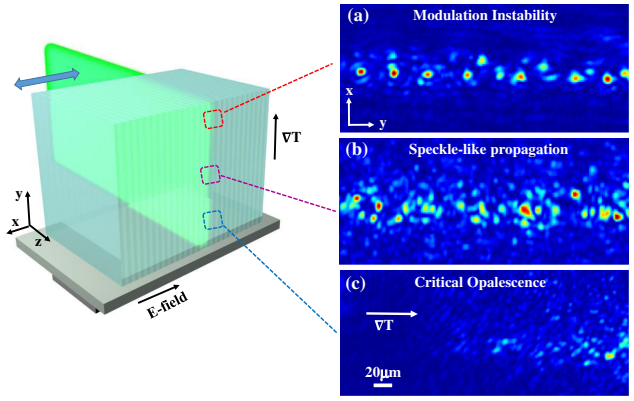

FIG. 1 (color online). Nonlinear beam propagation in photorefractive KLTN when an external electric field induces the ferroelectric phase transition. (left) Sketch of the experimental geometry and (right) different local propagation regimes selected by the thermal gradient. Transmission microscopy images revealing (a) modulation instability, (b) speckle-like propagation, and (c) critical opalescence.

point, corresponding to an effective local temperature that is exactly T_C. In this case, a disordered index of refraction pattern forms over spatial scales comparable with λ, introducing scattering and fragmentation in the nonlinear propagation, with the formation of narrower interacting filaments. What emerges is a disordered output intensity distribution $I(x, y)$ with micrometric spots of various intensity that is "speckle-like" [35].

In order to study the statistical properties of the speckle-like intensity pattern, we first quantify the intensity fluctuation amplitude in the spatial light distribution introducing the deviation $[I(x, y) - \langle I \rangle]/\langle I \rangle$ from the spatial mean value $\langle I \rangle$. Large deviations are observed in the disordered output of this highly nonlinear regime with the appearance of bright micrometric spots of extreme intensity. In Figs. 2(b)–2(c) we report, as an example, two measured speckle-like outputs with the associated fluctuations along a y direction in the insets; in Fig. 2(c) we show an instance of an extreme event, spatially localized, with a peak intensity of approximately twenty times larger than the averaged intensity. The measured transverse dimension (FWHM) of this exceedingly bright microbeam is 3 μm. Further analysis reported hereafter indicates this event as a rogue wave.

The disordered pattern with rogue fluctuations is observed at steady state after an initial transient stage that lasts $t \approx 10$ s for the μW beam power used. During the transient, the beam diffracts in an inhomogeneous setting, associated with linear sample disorder, as it reaches the crystal output facet. The typical spatial distribution in this

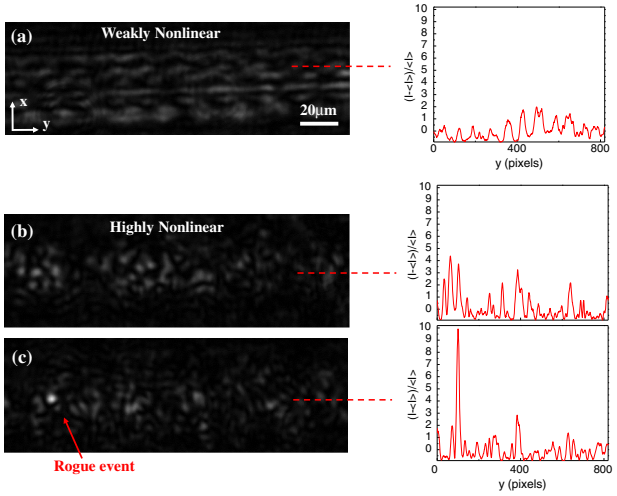

FIG. 2 (color online). Light intensity distribution transmitted through the biased photorefractive crystal exactly at critical condition. (a) Disordered pattern in the weakly nonlinear regime with the inset showing spatial intensity fluctuations along the red dashed y line. (b)–(c) Speckle-like pattern in the highly nonlinear regime, where the effect of large intensity fluctuations strongly affects the nonlinear dynamics. (c) An observation involving a bright spot with extreme intensity (approximately 20 times the averaged intensity), specified as rogue event.

"weakly" nonlinear regime is shown in Fig. 2(a), with the inset showing the smaller intensity fluctuations in this condition. This regime is superseded at subsequent times by the appearance of modulation instability and breakup, where disorder appears to have a dynamic and strongly amplified effect on light, which then leads to the final steady-state highly nonlinear regime, at $t \approx 100$ s, where rogue waves are detected. This transient nature is related to the physics of the photorefractive nonlinearity, which involves a buildup of a photogenerated space-charge field, so that the beam-induced index of refraction modulation accumulates in time. Once the steady condition has been reached, the beam continues to experience stationary continuous spatiotemporal fluctuations associated to the nonequilibrium features and long-range correlations in the refractive index at the Curie point. So we observe the specklelike pattern to vary dynamically under the action of different disorder configurations [27].

In fact, we have acquired a large set of uncorrelated images (approximately 10^3) in the same experimental conditions but with different intrinsic disorder landscapes. Histograms of the intensity values in a transverse region of the image for linear and nonlinear propagation then allow us to measure the corresponding probability distribution functions $P(I)$. Results are shown in Fig. 3, where the intensity statistics observed for the highly nonlinear specklelike pattern is compared to that observed for the weakly nonlinear regime. In both cases the incoherent part is of the order of the background intensity I_b and is not shown [35]. Long-tail statistics characterize the steady-state highly nonlinear condition, as reported in Fig. 3(a). The experimental behavior strongly deviates from a Gaussian distribution, which implies a decay according to $P(I) = \exp(-I/\langle I\rangle)/\langle I\rangle$ that we have evaluated with the measured

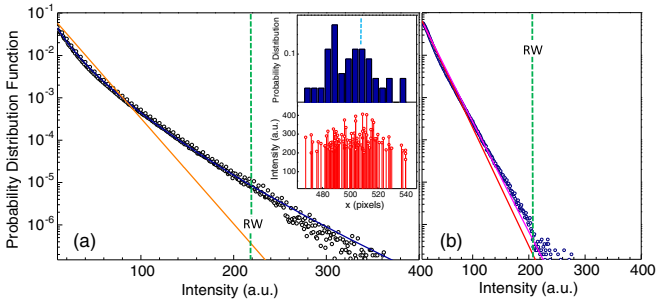

FIG. 3 (color online). Intensity distribution statistics. (a) Long-tail statistics in the highly nonlinear regime: experimentally revealed (black circles), fitting function (blue line), and consistent Gaussian distribution for comparison (orange line). The inset shows the spatial x position of several observed rogue events (bottom) with the corresponding counts histogram (top). (b) Gaussian statistics in the weakly nonlinear regime: experimentally revealed (blue circles), fitting function (magenta line) and consistent Gaussian distribution for comparison (red line). The vertical green dotted lines indicate the rogue waves (RW) thresholds.

$\langle I\rangle$ value (orange line) [14,35]. In particular, the observed intensity distribution is well fitted by a stretched exponential decay (blue line) in the form of $P(I) = \exp(-cI^b - a)$. The stretching parameter b quantifies the deviation from Gaussianity and long-tailed behavior is indicated by $b < 1$ [36]. We obtain $b = 0.65 \pm 0.02$, demonstrating that extreme intensity occurs with heavy probability. To further analyze the "rare" events, we calculate the significant wave height, defined as the mean amplitude of the highest one third of detected waves. Events of amplitude exceeding at least by a factor of 2 this value are commonly referred to as rogue waves (hydrodynamic threshold) [2,3]. Setting the threshold in Fig. 3 (green dotted line) we identify a large number of events as spatial rogue waves, among which is the one reported in Fig. 2(c). The extension of such oceanographic criterion, which is associated to the wave amplitude, to our optical system, where we observe the envelope intensity pattern, is here validated by the fact that the threshold approximately coincides with the end of the normal statistics. Taking several recorded extreme events, we then consider the spatial point at which they appear to achieve information on the role of anisotropic field effects in their generation. Counts as a function of the peak transverse x position are reported in the inset of Fig. 3(a); the distribution is qualitatively centered near the beam averaged midpoint (blue reference line) without a shifted prevailing component. This means that in our system the effect of self-bending, associated to diffusive and displacement fields, plays a negligible role in the emergence of rogue waves. This is an intriguing finding since these effects are, in the spatial domain, the counterpart of Raman shift in optical fiber propagation [37] and rogue temporal events are usually associated with the most redshifted soliton in supercontinuum generation [38–41]. Here, the spatial lateral shift (along x) is observed for the whole beam profile and it amounts approximately to 20 μm at the crystal output. Results in the weakly nonlinear regime are reported in Fig. 3(b). The statistical distribution loses its long tail in this case, showing only a small deviation from the Gaussian behavior, evaluated as previously (red line). For comparison with the highly nonlinear case, we fit the detected data with $P(I) = \exp(-cI^b - a)$ (magenta line). The stretching exponent is now close to one, $b = 0.99 \pm 0.07$, confirming the normal scenario. This fact is quite interesting since it implies that, through the strength of the nonlinear interaction, long-tail statistics can be deterministically generated and controlled. It also associates a fundamental role to the nonlinear response in the appearance of rogue waves.

To grasp the origin of each single rogue event and how the amount of nonlinearity can affect microscopically its formation, we perform a numerical $(2+1)$D split-step Fourier method analysis of the generalized nonlinear Shrödinger equation describing the paraxial spatial evolution of the optical field envelope $A(x, y, z)$ in

centrosymmetric photorefractive media. Considering the leading terms in the model, the nonlinearity contains a Kerr-saturated component and a saturated Raman-like component due to the charge diffusive field and reads [32]

$$i\partial_z A = -\frac{1}{2k}\nabla_\perp^2 A + \frac{k}{n}\Delta n(\bar{I})A, \quad (1)$$

$$\Delta n(\bar{I}) = \frac{1}{2}n^3 g\varepsilon_0^2\chi^2\left[\frac{E_0^2}{(1+\bar{I})^2} - a\frac{\nabla\bar{I}}{(1+\bar{I})^2}\right]. \quad (2)$$

Here, $\bar{I}$ is the intensity normalized to the background ($\bar{I} = |A|^2/I_b$), $k = 2\pi n/\lambda$ the wave number, n the refractive index, a the diffusive nonlinear parameter, $E_0 = V/l_x$ the bias field and χ the dielectric susceptibility, coupled to the electric field via the electro-optical coefficient g. Following previous studies in the temporal domain [38], the regime of intense filament formation was found from Eqs. (1) and (2), adding a spectrally random seed noise to the input Gaussian beam. Scattering during propagation was found numerically to not alter these single rogue wave kinematics and only weakly affect the high-intensity statistical properties of the field, and was rendered negligible. This means that, although in experiments turbulence associated to the out-of-equilibrium state of the medium is a key ingredient to trigger extreme events, in numerics, where such turbulence-mediated disorder is absent, input disorder amplification is sufficient to generate rogue waves. The values of the parameters are selected so as to match those for the KLTN sample and optical setup, except for χ, that is the parameter through which we fix the strength of the nonlinearity. In details, we have $\bar{I} = 30$, $n = 2.4$, $g = 0.16\ \mathrm{m}^2/C^4$, $E_0 = 2\times10^5$ V/m and a weakly intensity-dependent absorption is used, with average value $\alpha = 2\ \mathrm{cm}^{-1}$; moreover, the susceptibility χ is known assuming local giant values, of the order of 10^5, during the phase transition in similar photorefractive ferroelectric crystals [26,31]. Results are in good agreement with the experimental kinematics of intense light filaments and show how, due to the strong nonlinear response, instabilities grow up during propagation eventually leading to the breaking of the beam waveform. We are able to identify two distinct regimes increasing the nonlinearity: the first condition precedes the onset of modulation instability, while the second is characterized by randomic solitons fusion. In Fig. 4 are reported a simulated beam propagation in both cases, respectively, with $\chi = 5\times10^4$ and $\chi = 10^5$. We find multisoliton formation in the highly nonlinear conditions [Fig. 4(b)]; here, collisions and mergers dynamically lead to an intensity distribution with larger spatial fluctuations [Fig. 4(c)] and localized structures with giant amplitudes emerge. As shown in Fig. 4(d), the output probability distribution function reveals a characteristic long-tailed behavior in good agreement with the experimental statistics and confirms the rogue waves scenario. Moreover, consistently

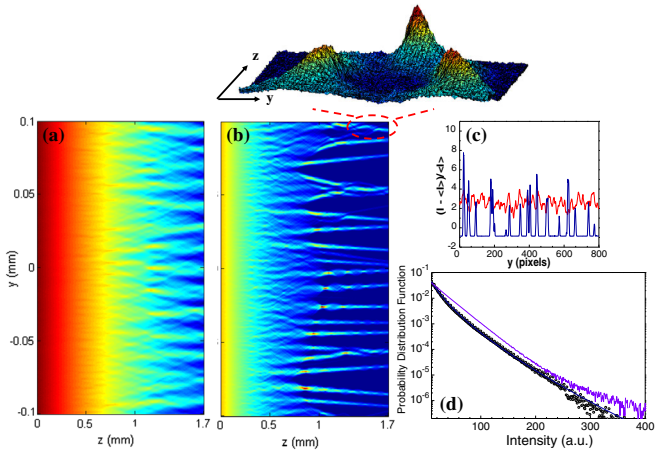

FIG. 4 (color online). Numerical simulations of the beam intensity evolving along the propagation z direction. Typical wave dynamics in the $y-z$ section in (a) nonlinear conditions ($\chi = 5\times10^4$) and (b) highly nonlinear conditions ($\chi = 10^5$), where soliton collisions and mergers take place leading to giant peak intensities (detail in the inset). (c) Comparison between output deviations in (a) and (b) along y. (d) Numerical long-tail statistical distribution in the highly nonlinear regime (purple line) compared with the experimental data.

with the experiments, such scenario of nonlinear origin results weakly affected by the Raman-like component in Eq. (2). In particular, the simultaneous occurrence of interaction processes and extreme intensity fluctuations suggest that filament mergers may be the microscopic mechanism at the basis of extreme intensity waves. Recent studies in multifilamentation [15] and in optical fiber [38] have also pointed out a similar conclusion, and this places our results in a general context that may relate rogue waves to turbulence phenomena in systems described by a nonintegrable nonlinear Shrödinger model [42].

To further investigate the role of soliton mergers in rogue waves' appearance, we analyzed the extreme intensity spots in terms of soliton physics, casting the normalized width or amplitude of the filaments in the soliton parameter plane. Considering the reduced $(1+1)$D model, soliton solutions of the type $A(x,z) = u(x)e^{i\Gamma z}\sqrt{I_b}$ must satisfy specific existence conditions [32,43], expressed in terms of the normalized input peak amplitude $u_0 = \sqrt{\max\{\bar{I}\}}$ and soliton FWHM $\Delta\xi = \Delta x[kn\sqrt{g}\varepsilon_0]\chi E_0$ (soliton existence curve). The observed $(u_0, \Delta\xi)$ values for a set of rogue waves are reported in Fig. 5 and compared to the theoretical soliton existence conditions. The experimental points are analyzed assuming a constant $\chi = 10^5$, coherently with the numerical simulations. Two facts are evident. First, the filaments do, in fact, fall in proximity of the existence conditions, even though a single averaged value of effective χ is used. Second, the filaments appear to populate the highly saturated region of the soliton existence curve. The first fact confirms the role played by instabilities in giving rise to general complex spatial structures of solitons [27].

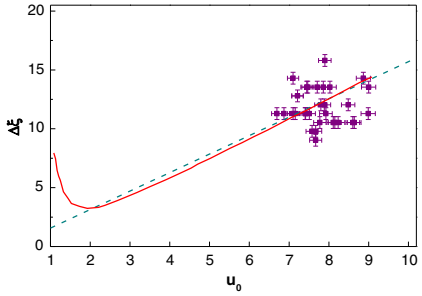

FIG. 5 (color online). Existence conditions for Kerr-saturated solitons. Observed extreme events (purple points), linear asymptotic behavior predicted by wave harmonic theory [37] (dashed blue line), and exact (numeric) existence conditions [32] (red line).

The second suggests a role played by scale invariance. In fact, in highly saturated conditions ($u_0 \gg 1$), solitons are known to manifest self-similarity in the form of a scale-invariance relationship $A(x,z) \to q^{-1}A(qx,q^2z)$ [44]. Remarkably, scale invariance is one of the fundamental ingredients thought to play a key role in the emergence of extreme events with heavy probabilities, as occurs for disordered fields through the integration over multiple spatial scales and in the long-correlated random model [45].

To conclude, we report the first observation of optical spatial rogue waves and their long-tail statistics in a nonlinear optical crystal. The result is found in the disordered Kerr-saturated solitonlike propagation occurring in a biased photorefractive ferroelectric KLTN undergoing a phase transition. Superresolved micrometric bright spots with intensity more than 20 times that of the average is observed. Changing the strength of the nonlinearity allows us to suppress on command deviations from Gaussianity. The extreme events are microscopically related to mergers of solitons and, in future works, a nonlinear series analysis can be developed to study correlation and predictability of such microscopic processes [3]. Scale invariance of the soliton solutions further elucidate the physical picture, explaining the occurrence of waves with arbitrary large intensity. Our results open new important possibilities for observing rogue waves in new systems, such as different nonlinear optical crystals. At the same time, they lead to a more profound understanding with respect to the debated role of nonlinear interaction in the appearance and control of long-tail statistics.

Funding from PRIN Grants No. 2012BFNWZ2, and Sapienza Awards Project are acknowledged.

*Davide.Pierangeli@roma1.infn.it

[1] M. Onorato, S. Residori, U. Bortolozzo, A. Montina, and F. T. Arecchi, Phys. Rep. **528**, 47 (2013).
[2] J. M. Dudley, F. Dias, M. Erkintalo, and G. Genty, Nat. Photonics **8**, 755 (2014).
[3] S. Birkholz, C. Brée, A. Demircan, and G. Steinmeyer, Phys. Rev. Lett. **114**, 213901 (2015).
[4] D. R. Solli, C. Ropers, P. Koonath, and B. Jalali, Nature (London) **450**, 1054 (2007).
[5] J. M. Dudley, G. Genty, and B. J. Eggleton, Opt. Express **16**, 3644 (2008).
[6] D. R. Solli, C. Ropers, and B. Jalali, Appl. Phys. Lett. **96**, 151108 (2010).
[7] B. Frisquet, B. Kibler, and G. Millot, Phys. Rev. X **3**, 041032 (2013).
[8] C. Lecaplain, Ph. Grelu, J. M. Soto-Crespo, and N. Akhmediev, Phys. Rev. Lett. **108**, 233901 (2012).
[9] C. Bonatto, M. Feyereisen, S. Barland, M. Giudici, C. Masoller, J. R. Rios Leite, and J. R. Tredicce, Phys. Rev. Lett. **107**, 053901 (2011).
[10] D. V. Churkin, O. A. Gorbunov, and S. V. Smirnov, Opt. Lett. **36**, 3617 (2011).
[11] A. Coillet, J. Dudley, G. Genty, L. Larger, and Y. K. Chembo, Phys. Rev. A **89**, 013835 (2014).
[12] K. Hammani, B. Kibler, C. Finot, and A. Picozzi, Phys. Lett. A **374**, 3585 (2010).
[13] A. N. Pisarchik, R. Jaimes-Reategui, R. Sevilla-Escoboza, G. Huerta-Cuellar, and M. Taki, Phys. Rev. Lett. **107**, 274101 (2011).
[14] F. T. Arecchi, U. Bortolozzo, A. Montina, and S. Residori, Phys. Rev. Lett. **106**, 153901 (2011).
[15] S. Birkholz, E. T. J. Nibbering, C. Brée, S. Skupin, A. Demircan, G. Genty, and G. Steinmeyer, Phys. Rev. Lett. **111**, 243903 (2013).
[16] A. Montina, U. Bortolozzo, S. Residori, and F. T. Arecchi, Phys. Rev. Lett. **103**, 173901 (2009).
[17] P. M. Lushnikov and N. Vladimirova, Opt. Lett. **35**, 1965 (2010).
[18] M. Leonetti and C. Conti, Appl. Phys. Lett. **106**, 254103 (2015).
[19] C. Liu, R. E. C. van derWel, N. Rotenberg, L. Kuipers, T. F. Krauss, A. Di Falco, and A. Fratalocchi, Nat. Phys. **11**, 358 (2015).
[20] R. W. Boyd, *Nonlinear Optics* (Academic, New York, 2003).
[21] L. Solymar, D. J. Webb, and A. Grunnet-Jepsen, *The Physics and Applications of Photorefractive Materials* (Oxford University Press, New York, 1996).
[22] E. DelRe, M. Tamburrini, M. Segev, R. Della Pergola, and A. J. Agranat, Phys. Rev. Lett. **83**, 1954 (1999).
[23] E. DelRe, E. Spinozzi, A. J. Agranat, and C. Conti, Nat. Photonics **5**, 39 (2011).
[24] D. Pierangeli, J. Parravicini, F. Di Mei, G. B. Parravicini, A. J. Agranat, and E. DelRe, Opt. Lett. **39**, 1657 (2014).
[25] F. Di Mei, J. Parravicini, D. Pierangeli, C. Conti, A. J. Agranat, and E. DelRe, Opt. Express **22**, 31434 (2014).
[26] E. DelRe, F. Di Mei, J. Parravicini, G. B. Parravicini, A. J. Agranat, and C. Conti, Nat. Photonics **9**, 228 (2015).
[27] C. Conti, Phys. Rev. E **72**, 066620 (2005).
[28] A. Agranat, R. Hofmeister, and A. Yariv, Opt. Lett. **17**, 713 (1992).
[29] T. Imai, S. Toyoda, J. Miyazu, J. Kobayashi, and S. Kojima, Appl. Phys. Express **7**, 071501 (2014).
[30] H. Tian, B. Yao, P. Tan, Z. Zhou, G. Shi, D. Gong, and R. Zhang, Appl. Phys. Lett. **106**, 102903 (2015).

[31] D. Pierangeli, F. Di Mei, J. Parravicini, G. B. Parravicini, A. J. Agranat, C. Conti, and E. DelRe, Opt. Mater. Express **4**, 1487 (2014).
[32] E. DelRe, B. Crosignani, and P. Di Porto, Prog. Opt. **53**, 153 (2009).
[33] A. V. Mamaev, M. Saffman, D. Z. Anderson, and A. A. Zozulya, Phys. Rev. A **54**, 870 (1996).
[34] D. Pierangeli, M. Flammini, F. Di Mei, J. Parravicini, C. E. M. de Oliveira, A. J. Agranat, and E. DelRe, Phys. Rev. Lett. **114**, 203901 (2015).
[35] J. W. Goodman, *Statistical Properties of Laser Speckle Patterns* (Springer, Berlin, Heidelberg, 1975).
[36] A. Clauset, C. R. Shalizi, and M. E. Newman, SIAM Rev. **51**, 661 (2009).
[37] E. DelRe, A. D'Ercole, and E. Palange, Phys. Rev. E **71**, 036610 (2005).
[38] A. Armaroli, C. Conti, and F. Biancalana, Optica **2**, 497 (2015).
[39] A. Demircan, S. Amiranashvili, C. Brée, C. Mahnke, F. Mitschke, and G. Steinmeyer, Sci. Rep. **2**, 850 (2012).
[40] L. G. Wright, W. H. Renninger, D. N. Christodoulides, and F. W. Wise, Opt. Express **23**, 3492 (2015).
[41] M. Conforti, S. Trillo, A. Mussot, and A. Kudlinski, Sci. Rep. **5**, 9433 (2015).
[42] P. Walczak, S. Randoux, and P. Suret, Phys. Rev. Lett. **114**, 143903 (2015).
[43] J. Parravicini, D. Pierangeli, F. Di Mei, C. Conti, A. J. Agranat, and E. DelRe, Opt. Express **21**, 30573 (2013).
[44] E. DelRe, A. D'Ercole, and A. J. Agranat, Opt. Lett. **28**, 260 (2003).
[45] G. Parisi, *Statistical Field Theory* (Addison-Wesley, New York, 1988).